



Wash-free 3D imaging and detection of glioma with a novel neuropotential targeted AIE probe†

Cite this: *Chem. Commun.*, 2021, 57, 801

Received 4th November 2020,
 Accepted 11th December 2020

DOI: 10.1039/d0cc07289c

rsc.li/chemcomm

Junyong Wu,^{‡a} Anyao Bi,^{‡b} Fan Zheng,^b Shuai Huang,^b Yongjiang Li,^a
 Jipeng Ding,^{id b} Daxiong Xiang^{*a} and Wenbin Zeng^{id *b}

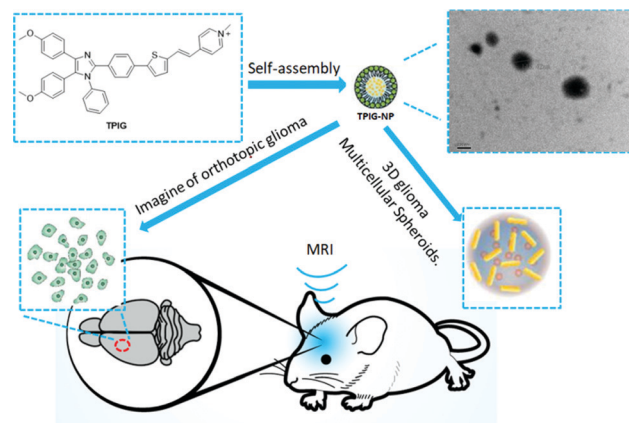
We herein developed a novel tetraarylimidazole-based AIE probe TPIG-NP to selectively image and quantitatively detect glioma. Due to the distinct negatively charged glioma cells, TPIG-NP with an opposite charge could achieve wash-free imaging of glioma cells and 3D multicellular spheroids.

Gliomas comprise a group of heterogeneous primary brain neoplasms, accounting for 81% of central nervous system (CNS) malignancies.^{1,2} They can be further categorized into four grades based on the classification of the World Health Organization (WHO). The first two grades indicate low-grade glioma (LGG), while the latter two are high-grade glioma (HGG).³ Typically, a relatively high grade is related to a poor prognosis. The median survival time of LGG is 11.6 years, whereas glioblastoma (GBM), the most common type of grade 4 gliomas, has a median overall survival time of only 1.2 years.^{4,5} Due to the diffuse dissemination of glioma cells, complete excision of all tumour regions is almost impossible, resulting in poor prognosis. Therefore, imaging is often required for the detection of glioma infiltration during surgery.

Advances in various imaging technologies, such as ultrasound, computed tomography (CT), and magnetic resonance imaging (MRI), have made great contributions in glioma detection.^{6,7} Compared with these techniques, detection using fluorescent probes possesses the ability of highly sensitive imaging and real-time visualization so that it can precisely visually distinguish glioma from the normal brain tissues more easily.^{8–11} However, to achieve a high signal-to-background ratio, a washing step is often required after incubation with the probes to reduce the background fluorescence, which is not suitable for monitoring glioma *in situ*. Meanwhile, with a high

concentration solution or in the aggregate state, most of the conventional fluorophores are either weakly emissive or non-emissive, which has been known as the aggregation-caused quenching (ACQ) effect. Tang *et al.*, in *Chem. Commun.*, 2001, 18, 1740, reported a novel class of fluorophores with aggregation-induced emission (AIE) properties that solve the problems of the ACQ effect.¹² AIE luminogens (AIEgens) show little fluorescence in the dissolved state and significantly enhanced fluorescence in aggregates. It is based on the AIE characteristics that this type of probes is able to self-assemble into nanoparticles and can be used for wash-free cell imaging as well.

Recently, our group has focused on the design of AIE probes and built a tetraarylimidazole AIE parent nucleus **TPI**.^{13,14} Herein, in this study, we report a novel terpyridyl-based derivative nanoprobe **TPIG-NP** for the wash-free imaging of glioma cells and tissues (Scheme 1). As the electrical potential of glioma cells is significantly lower than those of the other tumour cells and normal brain cells, **TPIG-NP** with a positive charge can selectively be absorbed and enriched by glioma cells through electrostatic attraction. High fluorescent signals with



Scheme 1 Schematic illustration of a self-assembled nanoprobe (**TPIG-NP**) to exert imaging of glioma.

^a Department of Pharmacy, The Second Xiangya Hospital, Central South University, Changsha, 410011, China. E-mail: xiangdaxiong@csu.edu.cn

^b Xiangya School of Pharmaceutical Sciences, Central South University, Changsha, 410013, P. R. China. E-mail: wbzeng@hotmail.com

† Electronic supplementary information (ESI) available. See DOI: 10.1039/d0cc07289c

‡ These authors contributed equally to this work.

low background interference are then observed to image every single cell. In addition, the imaging capacity of the probe is also approved in the 3D multicellular spheroids of glioma cells and in brain tissues as well.^{15–19} No washing steps are required to remove any probes in this process, making **TPIG-NP** ideal for glioma assays *in vitro* and *in vivo*. It is hoped that **TPIG-NP** can further provide a robust sensing platform for guiding the precise resection of glioma and improving the prognosis of patients.

TPIG was synthesized *via* multiple steps as described in Scheme S1 (please see the ESI†). The AIE characteristic of **TPIG** was measured as shown in Fig. S3 (see the ESI†). The formation of monodisperse NPs was verified by transmission electron microscopy (TEM) analysis (see Fig. S5, ESI†). The optical properties of **TPIG-NP** are shown in Fig. S1–S3, ESI.†

To fully evaluate the performance of different functionals in modelling the TICT formations, we calculated the S0 PbE0, the S1 de-excitation energies (vertical emissions) and resulting S1 PbE0 in DMSO based on the optimized S1 molecular structures of **TPIG**. We also performed hole-electron analysis calculations on **TPIG** as a benchmark (Fig. 1a). Hole-electron analysis has been proved to be a reliable approach to including electron-hole effects and intramolecular charge transfer excitations (ICTs). It is clearly to find that the flow of electron in the exciting state of **TPIG** in holes is from the donor to the acceptor, demonstrating a typical ICT effect. It was reported that the crystal structure of the simple fluoresce in comprises a network of intermolecular avoid face-to-face π - π stacking.²⁰ No effective face-to-face π - π stacking interactions can be observed due to the steric spatial repulsion of the benzene group which was conjuncted to imidazole. Structure analyses revealed that the restriction of the face-to-face π - π stacking interactions of **TPIG** could be an effective approach to AIE. Electrostatic potential (ESP) attracted ongoing studies in the biological and medicinal chemistry literature because it can unravel the charge distribution of chemical molecules, which plays an important role in biological cases. After calculation analysing to the ESP of **TPIG** (Fig. 1b), the whole molecule possessed a positive charge,

indicating its potential of application in neural potential activity in biological events.²¹

Before applying **TPIG-NP** to image living cells, for safety concerns, we first evaluated its cytotoxicity against brain-derived endothelial cells.3 (bEnd.3) and human glioma cells (U87-MG, HS683, and T98 cells). As depicted in Fig. 1, **TPIG-NP** had little effect on the cell viability against the tested cell lines, making this nanoprobe a biocompatible probe for further cell studies (Fig. 2).

Encouraged by the right results in the MTT assay, we further explored its imaging capability towards different cells. Distinguishing tumour cells from the surrounding normal cells is the primary condition for precise surgical navigation. However, due to the infiltrative nature of malignant glioma, it was difficult to precisely visually differentiate the boundary of glioma. Alternatively, in order to investigate the potential of **TPIG-NP** in distinguishing glioma cells from the normal brain cells, bEnd.3 and other three glioma cells HS683, T98 and U251 were treated with 10 μ M **TPIG-NP** for 2 h. As can be seen from Fig. 3, little signal can be recorded in bEnd.3 upon excitation at 430 nm, while obvious yellow-green fluorescence was observed in HS683 cells.

Meanwhile, the imaging region was evaluated with a co-localization experiment in HS683 cells, in which DAPI, a commercially available nucleus tracker, was used as a reference. HS683 cells were incubated with **TPIG-NP** (10 μ M) at 37 °C for 2 h, followed by incubation with DAPI (2 μ g ml⁻¹) under the same conditions. The merged image showed that the yellow-green fluorescence from the probe hardly colocalized with the blue signal from DAPI (Fig. 3), illustrating that **TPIG-NP** had a good ability to stain the cell membrane and the cytoplasm of glioblastoma cells. Next, another two glioma cell lines (T98 and U87-MG) were also treated with **TPIG-NP** for 2 h, respectively. Their wash-free fluorescence images reflected the same phenomena as in HS683 cells (Fig. 3), proving **TPIG-NP** as an effective imaging probe for glioma cells.

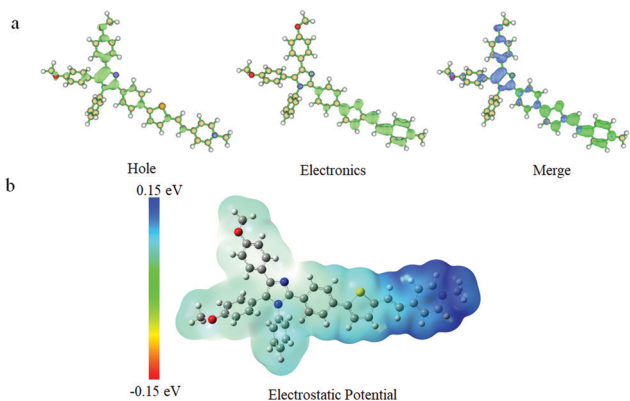


Fig. 1 (a) Distribution of holes and electrons of states calculated at PBE0/def2-TZVP in DMSO levels of theory *in vacuo*. (b). Electrostatic potential of TPIG.

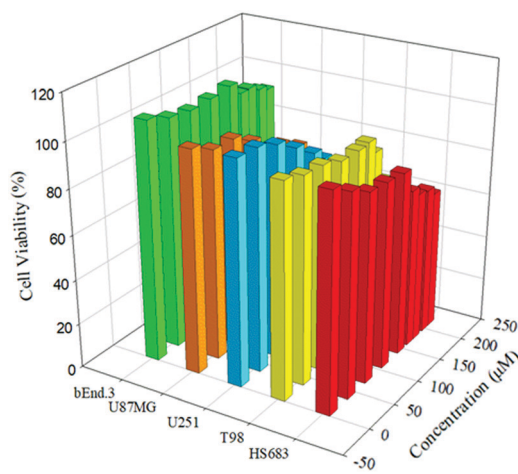


Fig. 2 (1). bEnd.3, (2). U87-MG cells, (3). U251 cells, (4). T98 cells, and (5). HS683 cells were separately treated with **TPIG-NP** for 4 h initially, and then cultured with a fresh medium for 72 h.

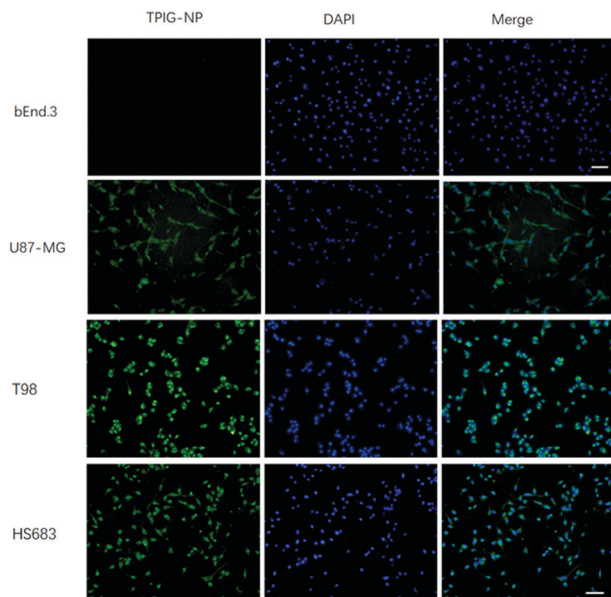


Fig. 3 Images of bEnd.3, U87-MG, T98 and HS683, respectively, treated with 10 μM TPIG-NP and DAPI (2 $\mu\text{g ml}^{-1}$) for 2 h by collecting the emissions at 530 nm upon excitation at 430 nm. Scale bar: 30 μm .

In order to further accurately identify and quantitatively detect the cells stained by TPIG-NP, we decided to combine flow cytometry (FCM) with fluorescence imaging which would be a more sensitive approach to characterize the probe in different cells. This could also eliminate some of the limitations demonstrated by conventional FCM, also providing morphological confirmation and distinguishing ability on brain cells as well. The bEnd.3 and glioma tumour cells were all treated with 10 μM TPIG-NP for 2 h, before FCM was performed. As shown in Fig. 5a, obviously, the mean fluorescence intensity (MFI) of bEnd.3 cell is 242, indicating that it had almost no fluorescence signal. On the other hand, as shown in Fig. 4a, all glioma cells (2, 3, 4, and 5) had nearly 10 fold (about 2×10^3 of MFI from FCM), in which high fluorescence signals were observed indicating the show-up of a great deal of glioma

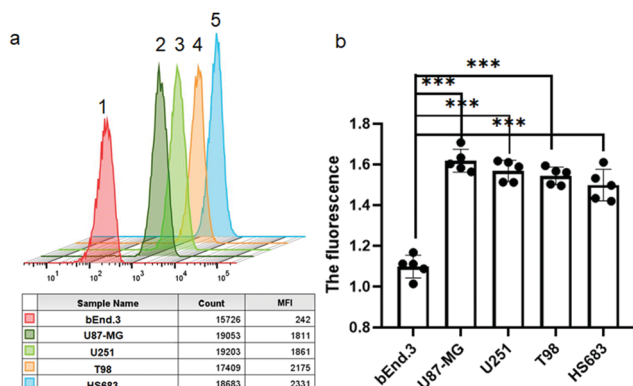


Fig. 4 (a) Accurate quantitative cell staining by flow cytometry, and each cell population was gated based on the intensity of SSC. ((1). bEnd.3, (2). U87-MG, (3). U251, (4). T98, (5). HS683). (b). The fluorescence intensity of various brain cell potentials. $p < 0.001$.

cells. These results intuitively reflected a significant difference of fluorescence between bEnd.3 and glioma tumour cells through the use of TPIG-NP. This further revealed that TPIG-NP could specifically image glioma cells among the brain cells which made it possible to apply TPIG-NP in auxiliary surgical resection of glioma. We hypothesized that it was the electrostatic attraction between the glioma cells and the probe that caused the highly selective imaging of TPIG-NP towards glioma cells.

Considering the results obtained from cell staining and flow cytometry assays, we then investigated the potential of the brain cells to find out the reason for the difference between the fluorescence imaging in the treatment groups. As depicted in Fig. 4b, the glioma cells (U87-MG, T98, U251, and HS683 cells) obviously possessed more negative cell potentials than bEnd.3 cell. These results implied that the higher electrostatic attraction of TPIG-NP with glioma induced highly selective imaging of the probe.

As oxygen concentration gradients always exist in the 350–500 μm 3D multicellular spheroids (MCSs), it makes the 3D MCSs the ideal models for the simulation of solid tumours at early stages. In this work, 10 μM of TPIG-NP was used for the MCSs of U87-MG cells which were developed for further evaluating the penetrative effect of the probe. After 2 h of incubation, strong yellow–green fluorescence signals were detected from the U87-MG MCSs (Fig. 5), indicating that TPIG-NP could easily penetrate into the sphere. Since the higher amount of the extracellular matrix components hampered the extracellular flow of the probe, the fluorescence of the outer layers of the spheroids was brighter, while lower signals were collected from the core part. These results confirmed that TPIG-NP had the potential to image glioma tumours.

To further evaluate the imaging performance of TPIG-NP *in vivo*, an orthotopic glioma mouse model was established through the injection of U87-MG cells into the brain (Fig. 6). T_1 -weighted magnetic resonance imaging (MRI) was applied to monitor the growth of glioma tumours. After 7 days of tumour

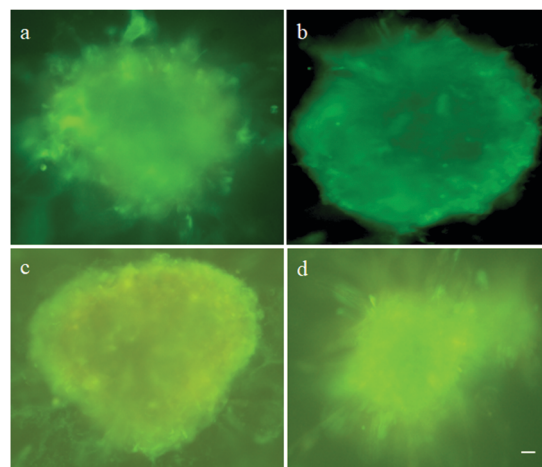


Fig. 5 Imaging of TPIG-NP in 3D glioma cell multicellular spheroids. ((a): U87-MG, (b): U251, (c): T98, (d): HS683.) Scale bar: 50 μm .

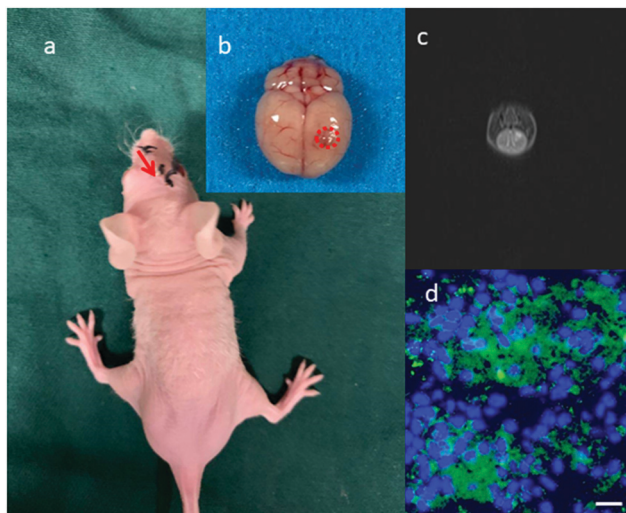


Fig. 6 (a) Preparation of orthotopic U87-MG glioma-bearing mouse. (b) *Ex vivo* images of the brain from orthotopic U87-MG glioma-bearing mouse. (c) MRI of the brain from orthotopic U87-MG glioma-bearing mouse. (d) Brain tissue section stained by using **TPIG-NP** (green light) and DAPI (blue light) of the brain from U87-MG glioma-bearing mouse. Scale bar = 50 μm .

cell inoculation, the tumour size in the brain was observed to be 6.35 mm^3 . Then, the brain tissue section was obtained. A strong **TPIG-NP** fluorescent signal (green light) was distributed in the tumour region rather than in the normal brain tissue, highlighting a clear tumour margin, which was consistent with the vivid boundary between the normal brain tissue and glioma detected by DAPI staining (blue light) (Fig. 6d). These results indicated that **TPIG-NP** was not only able to visualize tiny glioma but also able to detect the tumour margin.

To sum up, a new type of AIE probe **TPIG-NP** synthesized through the Suzuki coupling reaction was developed to image glioma *in vitro* and *in vivo*. Owing to its AIE characteristics, it could easily self-assemble into nanoparticles and provide strong fluorescence in aggregates. Meanwhile, no washing steps are required for **TPIG-NP** in the imaging process. Its obvious and selective imaging abilities were proved by different cell staining methods, flow cytometry assays, 3D MCSs, and a U87-MG glioma-bearing mouse model in sequence. As **TPIG-NP** was positively charged and a distinct negative charge was observed on glioma cells, the electrostatic attraction between the cells and the probe was responsible for high selectivity. It is expected that **TPIG-NP** could further be applied to precisely guide the resection of glioma in surgery.

This work was financially supported by the National Natural Science Foundation of China (81971678 and 81671756), the

Hunan Provincial Science and Technology Plan (2016TP2002), the Science and Technology Foundation of Hunan Province (2020SK3019, 2019SK2211 and 2019GK5012), and the Fundamental Research Funds for the Central Universities of Central South University (2018zzts041 and 2018dcyj067).

Conflicts of interest

The authors declare no competing financial interest.

Notes and references

- P. D. Delgado-López, P. Saiz-López, R. Gargini, E. Sola-Vendrell and S. Tejada, *Clin. Transl. Oncol.*, 2020, **22**, 1909.
- Q. T. Ostrom, H. Gittleman, G. Truitt, A. Boscia, C. Kruchko and J. S. Barnholtz-Sloan, *Neuro-Oncology*, 2018, **20**, 1.
- D. N. Louis, A. Perry, G. Reifenberger, A. von Deimling, D. Figarella-Branger, W. K. Cavenee, H. Ohgaki, O. D. Wiestler, P. Kleihues and D. W. Ellison, *Acta Neuropathol.*, 2016, **131**, 803.
- H. Ohgaki and P. Kleihues, *J. Neuropathol. Exp. Neurol.*, 2005, **64**, 479.
- P. D. Delgado-Lopez and E. M. Corrales-Garcia, *Clin. Transl. Oncol.*, 2016, **18**, 1062.
- M. Weller, M. van den Bent, J. C. Tonn, R. Stupp, M. Preusser, E. Cohen-Jonathan-Moyal, R. Henriksson, E. Le Rhun, C. Balana, O. Chinot, M. Bendszus, J. C. Reijneveld, F. Dhermain, P. French, C. Marosi, C. Watts, I. Oberg, G. Pilkington, B. G. Baumert, M. J. B. Taphoorn, M. Hegi, M. Westphal, G. Reifenberger, R. Soffietti and W. Wick, N.-O. European Assoc, *Lancet Oncol.*, 2017, **18**, e315.
- H. W. Davis, N. Hussain and X. Qi, *Mol. Cancer*, 2016, **15**, 33.
- W. T. Dou, L. F. Liu, J. Gao, Y. Zang, G. R. Chen, R. A. Field, T. D. James, J. Li and X. P. He, *Chem. Commun.*, 2020, **56**, 664.
- Y. Wen, F. J. Huo and C. X. Yin, *Chin. Chem. Lett.*, 2019, **10**, 1834.
- X. Luo, J. Li, J. Zhao, L. Y. Gu, X. H. Qian and Y. J. Yang, *Chin. Chem. Lett.*, 2019, **4**, 839.
- H. Y. Liu, G. Xu, T. L. Zhu, R. C. Wang, J. H. Tan, C. C. Zhao and X. F. Gu, *J. Mater. Chem. B*, 2020, 6013.
- J. D. Luo, Z. L. Xie, J. W. Y. Lam, L. Cheng, H. Y. Chen, C. F. Qiu, H. S. Kwok, X. W. Zhan, Y. Q. Liu, D. B. Zhu and B. Z. Tang, *Chem. Commun.*, 2001, 1740.
- X. Cao, T. Gao, J. Dong, X. Jiang, H. Zou, T. Liu, K. Yu and W. Zeng, *New J. Chem.*, 2019, **43**, 7874.
- S. Huang, T. Gao, A. Bi, X. Cao, B. Feng, M. Liu, T. Du, X. Feng and W. Zeng, *Dyes Pigm.*, 2020, **172**, 107830.
- Y. Huang, S. Wang, Q. Guo, S. Kessel, I. Rubinfeld, L. L.-Y. Chan, P. Li, Y. Liu, J. Qiu and C. Zhou, *Cancer Res.*, 2017, **77**, 6011.
- M. Zhu, Z. Sheng, Y. Jia, D. Hu, X. Liu, X. Xia, C. Liu, P. Wang, X. Wang and H. Zheng, *ACS Appl. Mater. Interfaces*, 2017, **9**, 39249.
- Y. J. Liu, H. H. Liu, H. X. Yan, Y. C. Liu, J. S. Zhang, W. J. Shan, P. X. Lai, H. H. Li, L. Ren, Z. J. Li and L. M. Nie, *Adv. Sci.*, 2019, **6**, 1801615.
- Y. J. Liu, Y. P. Yang, M. J. Sun, M. C. Cui, Y. Fu, Y. Lin, Z. J. Li and L. M. Nie, *Chem. Sci.*, 2017, **8**, 2710.
- Q. Yu, S. S. Huang, Z. Y. Wu, J. D. Zheng, X. Y. Chen and L. M. Nie, *J. Nucl. Med.*, 2020, **61**, 1079.
- M. Tremayne, B. M. Kariuki and K. D. M. Harris, *Angew. Chem., Int. Ed. Engl.*, 1997, **36**, 770.
- T. Lu and W. Chen, *J. Comput. Chem.*, 2012, **33**, 580.